Journal of Geophysical Research: Oceans

RESEARCH ARTICLE
10.1029/2017JC013653

Key Points:
- Spatial structure of oceanic ISV in the Philippine Sea is investigated with multisource observations and numerical simulations
- Mesoscale eddies and Rossby waves related to dynamic instability are major sources of oceanic ISV in the Philippine Sea
- MJO contributes half of the total observed ISV and acts in forming the ISV features in the Philippine Sea

Correspondence to:
S. Hu,
sjhu@qdio.ac.cn

Citation:
Hu, S., Sprintall, J., Guan, C., Sun, B., Wang, F., Yang, G., et al. (2018). Spatiotemporal features of intraseasonal oceanic variability in the Philippine Sea from mooring observations and numerical simulations. *Journal of Geophysical Research: Oceans, 123*, 4874–4887. https://doi.org/10.1029/2017JC013653

Received 23 NOV 2017
Accepted 15 JUN 2018
Accepted article online 26 JUN 2018
Published online 13 JUL 2018

Spatiotemporal Features of Intraseasonal Oceanic Variability in the Philippine Sea From Mooring Observations and Numerical Simulations

Shijian Hu[1,2,3,4,5], Janet Sprintall[6], Cong Guan[1,2,3,4], Bowen Sun[1,2,4], Fan Wang[1,2,3,4], Guang Yang[7,8], Fan Jia[1,3,4], Jianing Wang[1,3,4], Dunxin Hu[1,2,3,4], and Fei Chai[5,9]

[1]Key Laboratory of Ocean Circulation and Waves, Institute of Oceanology, Chinese Academy of Sciences, Qingdao, China, [2]University of Chinese Academy of Sciences, Beijing, China, [3]Laboratory for Ocean and Climate Dynamics, Qingdao National Laboratory for Marine Science and Technology, Qingdao, China, [4]Center for Ocean Mega-Science, Chinese Academy of Sciences, Qingdao, China, [5]State Key Laboratory of Satellite Ocean Environment Dynamics, Second Institute of Oceanography, State Oceanic Administration, Hangzhou, China, [6]Scripps Institution of Oceanography, University of California, San Diego, La Jolla, CA, USA, [7]Laboratory for Regional Oceanography and Numerical Modeling, Qingdao National Laboratory for Marine Science and Technology, Qingdao, China, [8]Center for Ocean and Climate Research, First Institute of Oceanography, State Oceanic Administration, Qingdao, China, [9]School of Marine Sciences, University of Maine, Orono, ME, USA

Abstract The Philippine Sea is located within the pathway of the propagating Madden-Julian Oscillation system and is also the destination for the North Pacific mesoscale oceanic eddies and waves. As such, the Philippine Sea is characterized by striking intraseasonal variability (ISV; 20–90 days) that plays a key role in bridging weather and climate. Spatial patterns and temporal features of intraseasonal oceanic variability along the Philippine coast are investigated using mooring observations and outputs from an eddy-resolving general circulation model. The amplitude of ISV determined from sea level anomaly is found to decrease from the northern and coastal Philippine Sea to the south and interior Pacific Ocean. In contrast, eddy kinetic energy features a northward decreasing gradient with a maximum at about 6°N. The meridional distribution of sea level anomaly and eddy kinetic energy spectra indicates that the ISV period increases with latitude and is symmetrical about the equator. Mesoscale eddies in the upper layer are tracked to explore the statistical distribution. Westward propagating mesoscale eddies and intraseasonal Rossby waves related to dynamic instabilities are an important source of the oceanic ISV in the Philippine Sea. Clear coastal propagation of ISVs related to coastal Kelvin waves is detected the south of about 14°N. Composite analysis shows that the Madden-Julian Oscillation is another important forcing shaping the spatial features of Philippine ISV intensity and contributes close to half of the observed total ISV.

1. Introduction

Intraseasonal variability (ISV; 20–90 days) plays a key role in bridging weather and climate (Zhang, 2013). The Philippine Sea is a place of abundant intraseasonal activities under the influence of oceanic processes such as mesoscale eddies, Kelvin waves, and intraseasonal long Rossby waves (e.g., Hu et al., 2013; Lin et al., 2005; Qiu et al., 2015, hereafter Qiu2015; Qu et al., 2012), as well as the coupled wind-precipitation Madden-Julian Oscillation (MJO) system (Madden & Julian, 1971, 1972; Wang et al., 2016). Along the Philippine coast, the Mindanao Current (MC) and Kuroshio redistribute the tropical water carried by the North Equatorial Current by strong meridional transports in opposing directions (Figure 1). Sparse observations suggest that both the MC and low-latitude Kuroshio have significant ISV (e.g., Hu et al., 2013; Kashino et al., 2005; Zhang et al., 2014). However, the spatial patterns and temporal features of intraseasonal variability in the Philippine Sea including the MC and Kuroshio region along the Philippine coast remain unclear due to a lack of systematic observations.

Individual investigations of the Kuroshio and subthermocline current below the MC indicate the importance of impinging energetic mesoscale eddies to the east of the Philippine islands (e.g., Gilson & Roemmich, 2002; Hu et al., 2013, 2015; Qiu et al., 2015; Wang, Zhai, & Hu, 2014; Wang, Zhai, Wang, & Hu, 2014; Zhang et al., 2014). Lin et al. (2005) suggested that ISV in the subtropical Pacific Ocean is mainly induced by free intraseasonal long Rossby waves. The MJO signal also propagates through the Philippine Sea and is expected to influence ISV phenomena in the region, although the exact effects remain uncertain. For example, Wang et al. (2016) pointed out that the ISV of zonal currents within 10°S–8°N is primarily caused by the MJO related atmospheric oscillation through wind forced baroclinic ocean waves, but Kashino et al. (2005) suggested that the

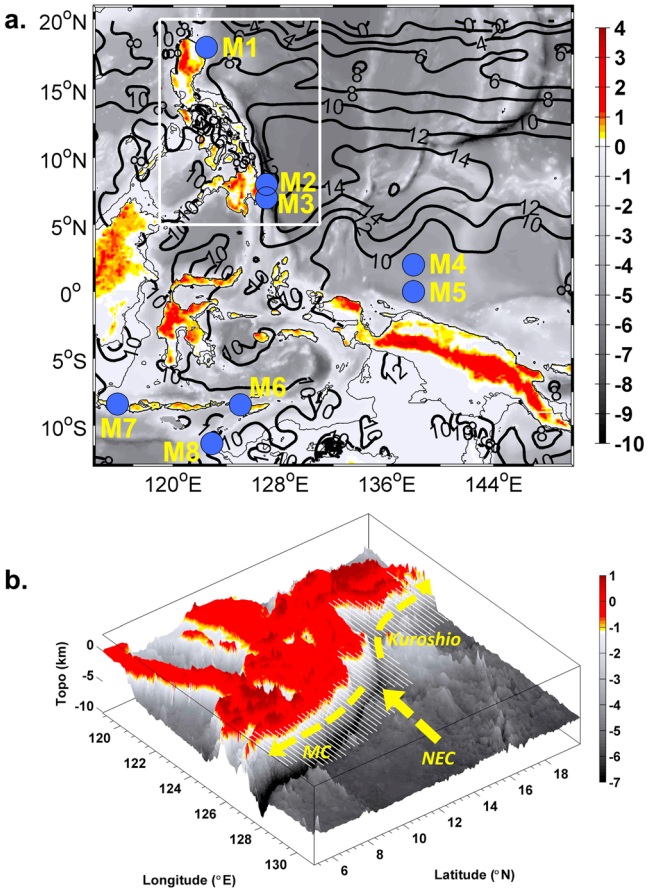

Figure 1. (a) Topography (color, kilometers) in the low-latitude western Pacific Ocean overlaid with annual mean sea level anomaly (black contour lines, unit in centimeters) over 2010–2013. Blue circles indicate locations of mooring observations used in this study. (b) Three-dimensional topography and sketch map of surface boundary currents to the east of the Philippine Islands denoted by the white box in (a). White lines mark the region extending 3° off the Philippine coast. NEC = North Equatorial Current; MC = Mindanao Current.

ISV of the MC was not well correlated with the atmospheric ISV. In addition, coastal Kelvin waves in this region (e.g., Liu et al., 2011; Zhuang et al., 2013) are expected to play a role in the ISV of MC and Kuroshio, but this has been rarely investigated. Therefore, the source and mechanisms that determine the spatial pattern of oceanic ISV in the Philippine Sea and the dynamical link of the coastal ISV in the MC and Kuroshio are still unsolved puzzles.

During the past two decades, in situ observations of the northwestern Pacific Ocean circulations have sharply increased due to international efforts like the Northwestern Pacific Ocean Circulation and Climate Experiment project (Hu et al., 2011), Tropical Atmosphere Ocean/Triangle Trans-Ocean Buoy Network project (McPhaden et al., 2009), and Argo program (Roemmich et al., 2009). In addition, direct observations of western boundary currents (WBCs) using Acoustic Doppler Current Profilers (ADCPs) have been collected (Figure 1a) and provide an opportunity to investigate the ISV of WBCs including the MC and Kuroshio.

This paper aims to map out the spatial pattern and temporal feature of the ISVs in the Philippine Sea with emphasis on the MC and Kuroshio along the Philippine coast using multisource mooring observations and numerical simulations combined with historical observations. The underlying dynamics that form the spatial structure of oceanic ISVs in the Indo-Pacific are investigated as well. In the following, we will describe the data sets in section 2. Results including temporal and spatial features, sources of these oceanic ISVs, and discussion of the role of MJO phenomena are presented in section 3. A summary is given in the last section.

2. Data Sets

We combine observational data sets with model outputs of the oceanic general circulation model for the Earth Simulator (OFES; Sasaki et al., 2008). Observations include daily ADCP velocities from five moorings from the Northwestern Pacific Ocean Circulation and Climate Experiment program (M1: 18°N, 122.5°E; M2: 8°N, 127°E) and the Tropical Atmosphere Ocean/Triangle Trans-Ocean Buoy Network (M3: 8°N, 127°E; M4: 2°N, 138°E; M5: 0°N, 138°E), and volume transports from the International Nusantara Stratification and Transport program (M6: Ombai Strait; M7: Lombok Strait; M8: Timor Passage; Sprintall et al., 2004). These moorings were chosen as they span the tropics and hence enable detection of any hemispherical asymmetry in ISV. Depth ranges of velocity measured by the ADCP on moorings M1 to M5 are shown in Figure 3. Method and quality control processing of the ADCP data and International Nusantara Stratification and Transport data has been previously detailed (Hu et al., 2013, 2016; Sprintall et al., 2009).

Argo products, including the Roemmich-Gilson Argo Climatology (Roemmich & Gilson, 2009) and the Absolute Geostrophic Velocity data derived from the Argo profiling observations (Gray & Riser, 2014), are also used. The RG Argo Climatology are monthly mean gridded (1° ×1°) temperature and salinity fields estimated using Argo profiles. The Absolute Geostrophic Velocity data derived from the Argo profiling observations provide quasi-global absolute geostrophic velocities of the upper 2,000 dbar of the ocean with a horizontal resolution of 1° and 29 regular pressure levels.

A number of remotely sensed data products are employed. The delayed time merged daily gridded sea level anomaly (SLA) during 2011–2013 are produced by the Data Unification and Altimeter Combination System and distributed by the Archiving, Validation, and Interpretation of Satellite Data in Oceanography/Centre National d'Etudes Spatiales (Dibarboure et al., 2009). In addition, satellite observation-based daily outgoing long-wave radiation (OLR), sea surface temperature (SST), and QuikSCAT wind stress curl are analyzed to

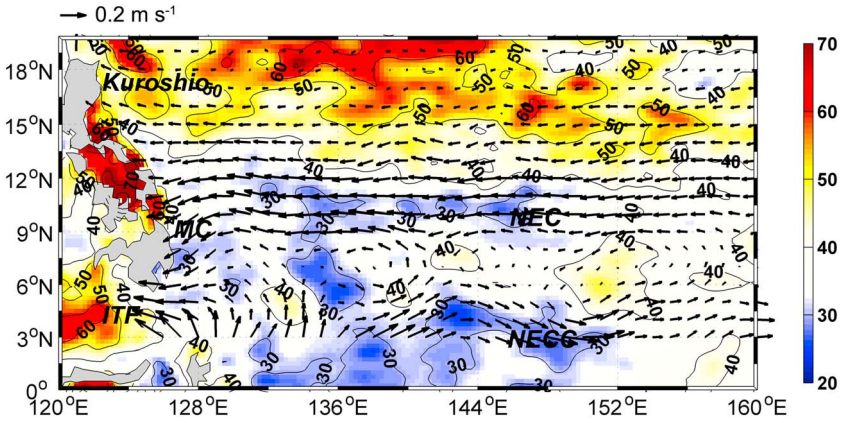

Figure 2. Annual-mean ratio (color, percentage) of the standard deviation of the intraseasonal SLA relative to standard deviation of SLA and overlaid with annual mean geostrophic current at 100 dbar (arrows) from the Absolute Geostrophic Velocity data derived from the Argo profiling observations data averaged over the period 2005–2010. SLA = sea level anomaly; MC = Mindanao Current; NEC = North Equatorial Current.

investigate the ISV processes. OLR data are provided by the National Oceanic and Atmospheric Administration (NOAA) Interpolated OLR data set from the National Center for Atmospheric Research archives based on Satellites NOAA16 and NOAA14 (Liebmann & Smith, 1996). SST are from the NOAA High-resolution Blended Analysis based on the Advanced Very High Resolution Radiometer infrared satellite SST data with a spatial grid resolution of 0.25° and a temporal resolution of 1 day (Reynolds et al., 2007). The Real-time Multivariate MJO index (Wheeler & Hendon, 2004) provided by the Bureau of

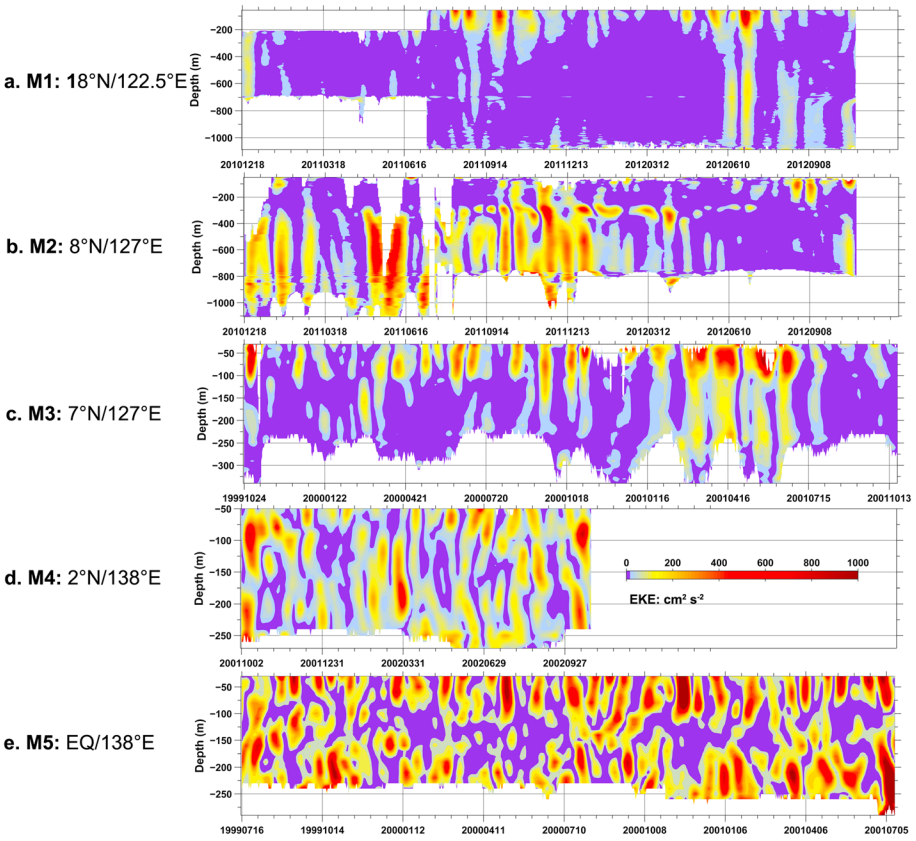

Figure 3. Time series of *EKE* ($cm^2\ s^{-2}$) observed by mooring Acoustic Doppler Current Profilers. See text for definition of the *EKE*. *EKE* = eddy kinetic energy.

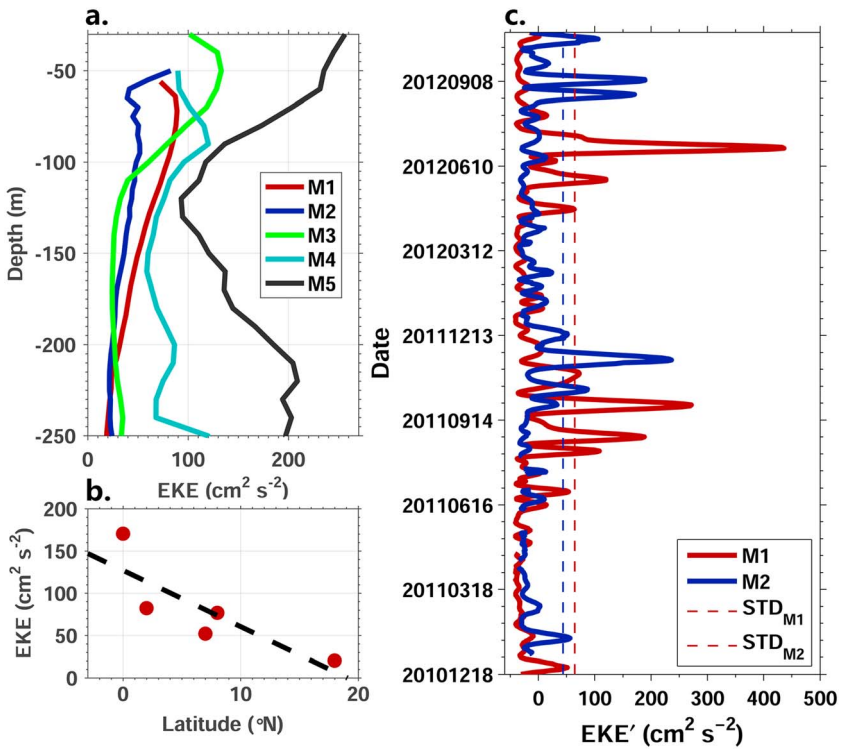

Figure 4. Vertical distribution of (a) mean *EKE* (cm^2 s^{-2}) and (b) upper 250-m layer mean *EKE* (dots) observed by mooring Acoustic Doppler Current Profilers. Dashed black line denotes the linear fit of upper layer *EKE* as a function of latitude. (c) Comparison of 0- to °400-m vertical mean *EKE*′ at M1 (18°N) and M2 (8°N), where dashed lines indicate standard deviations of the observed *EKE*′. *EKE* = eddy kinetic energy.

Meteorology of Australian Government is used to diagnose the MJO related processes (http://www.bom.gov.au/climate/mjo/graphics/rmm.74toRealtime.txt).

The OFES simulations has an eddy-resolving resolution of 0.1° in the horizontal and 54 levels in vertical direction. It was forced by the National Center for Environmental Prediction-National Center for Atmospheric Research reanalysis and is available for the period after 1980 at the Asia-Pacific Data-Research Center of the Hawaii University (http://apdrc.soest.hawaii.edu/data/data.php). In this study, the 3-day simulations during 2011–2013 are analyzed.

3. Results

3.1. Temporal and Spatial Features

The significance of ISV can be assessed by calculating the percentage ratio of standard deviation of intraseasonally filtered SLA relative to that of the raw SLA. As shown in Figure 2, the ISV is found in a large proportion of the Philippine Sea: 20% to 70% generally and 40% on average. Hence, the ISV is of significant importance for the low-latitude Pacific WBC region. In the coastal region, the ISV contributes about 47% of the total oceanic variability in the Kuroshio and MC region. ISV shows a greater proportion in the northern Philippine Sea than in the southern region.

Vertical and latitudinal distribution of the ISV is examined using moored ADCP observations and OFES model outputs. We calculate the eddy kinetic energy (*EKE*) by $EKE = \frac{1}{2}\left(u'^2 + v'^2\right)$, where u' and v' are intraseasonal time series of zonal and meridional velocity anomalies using a 20- to 90-day band-passed filter. Figure 3 presents a depth-time plot of *EKE* observed at M1 to M5 mooring sites, but note that the depth ranges and deployment dates are different among these moorings. In the surface layer (upper 400 m), *EKE* at the most northern mooring sites (M1 and M2) is weaker than that at the southern mooring sites (M4 and M5). However, in the subthermocline layer (about 400–1,000 m), M2 shows a much stronger *EKE* signal than in

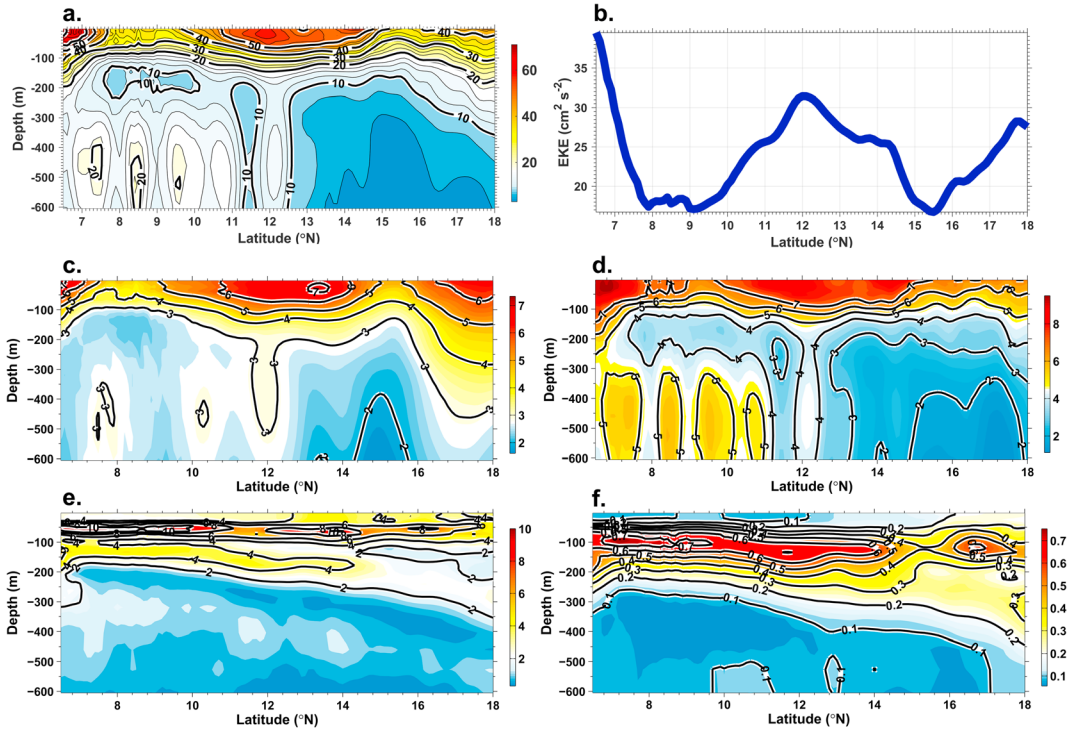

Figure 5. Coastal distribution of (a) annual mean *EKE* (cm^2 s^{-2}) and its (b) vertical mean over the 0- to 250-m layer, and standard deviations of coastal ISVs of (c) meridional velocity (cm s^{-1}), (d) zonal velocity (cm s^{-1}), (e) temperature (°C), and (f) salinity along the east coast of the Philippines. ISVs are calculated using a 20- to 90-day band-pass filter of OGCM for the Earth Simulator 3-day output and averaged over the 3° band off the Philippine coast (see Figure 1b). ISV = intraseasonal variability; *EKE* = eddy kinetic energy.

the surface layer. Standard deviations of *EKE* at M1 to M5 are 52, 70, 61, 93, and 210 cm^2/s^2, respectively; thus, the amplitude of the upper layer *EKE* is less than about 100 cm^2/s^2 for the mooring sites M1 to M4, but double that (about 200 cm^2/s^2) for M5. Among these moorings, M1, M2, and M3 are along the Philippine coast (Figure 1a), and their averaged *EKE* standard deviation is 61 cm^2/s^2. In the upper 250-m layer, in general, a linear decreasing gradient of *EKE* occurs from the equator toward the subtropics: *EKE* at M5 is greater than M4, and that is greater than at M3, M2, and M1 (Figures 4a and 4b).

Since the M1 and M2 were deployed concurrently, a comparison between them is also shown in Figure 4c. The correlation coefficient between EKE' at M1 and M2 is about −0.12. Significant ISV events ($EKE' > STD_{EKE}$) were detected in August–September, September–October, and October–November of 2011, and May and June–July of 2012 at M1. For M2, ISV events were observed in January and October–December of 2011 and August–October of 2012.

Annual mean *EKE* and ISV signals of current and temperature along the Philippine coast (out to 3°, Figure 1b) are examined using the OFES model output (Figure 5). Coastal ISVs are obviously concentrate in the upper layer above the thermocline, but different ISV features are evident for various variables: ISVs of meridional velocity and temperature shoal from the northern to southern Philippine Sea, but the *EKE* and ISV of zonal velocity shows equivalent features meridionally along the coast. The ISV of zonal velocity in the subsurface layer below 400 m is also significant south of about 13°N probably due to the existence of subthermocline eddies to the east of the Mindanao Island. This leads to a clear peak of *EKE* below 400 m and south of about 13°N. The maximum ISV of the currents occurs in the near-surface layer above 100 m, but the maximum ISV of temperature and salinity is at a depth of about 100 m (Figure 5).

The horizontal pattern of oceanic ISVs in the Philippine Sea is investigated using satellite observations of SST and SLA. Figure 6 presents the standard deviations of intraseasonal SST anomaly and SLA. The basic pattern is a southward decreasing gradient in standard deviations of SLA and SST in the Philippine Sea near the coast, with two standard deviation cores located to the east of Luzon and Mindanao Islands (Figure 6). SST standard

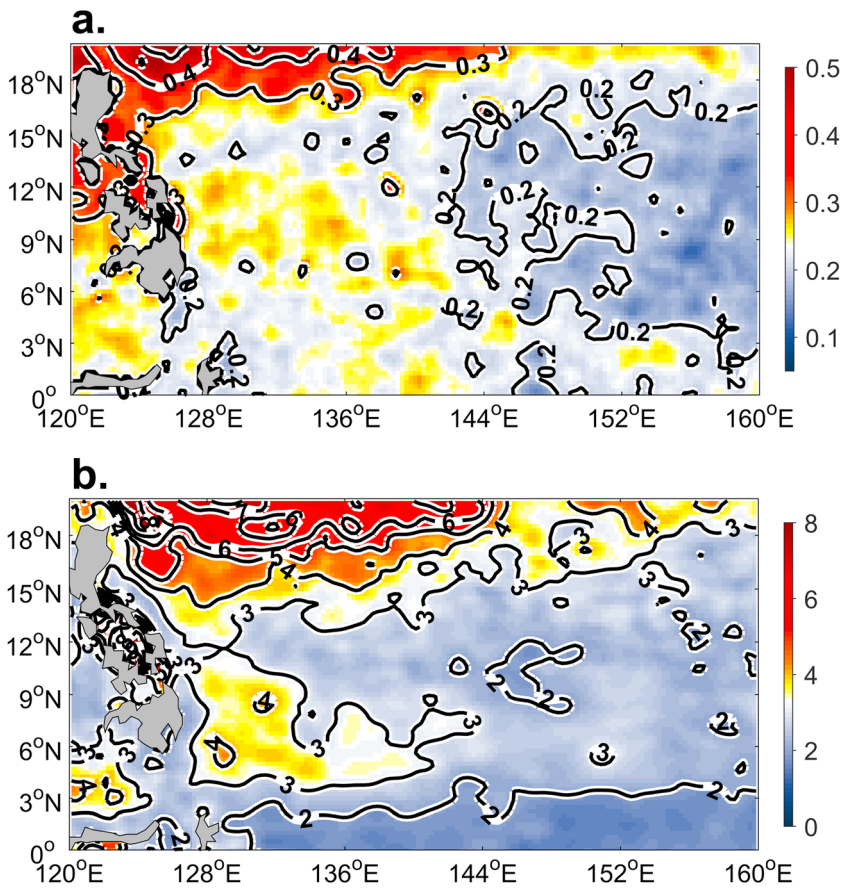

Figure 6. Standard deviations of sea surface temperature intraseasonal variability (a, °C) and sea level anomaly intraseasonal variability (b, cm) from satellite observations.

deviations is greater than 0.3 °C to the north of 15°N but less than 0.2 °C in the southern Philippine Sea. SLA standard deviation is about 4 to 8 cm in the northern Philippine Sea and decreases to 2 to 3 cm in the south. A secondary peak of SLA and SST standard deviations is located at about 9°N, of about 4 cm and 0.25 °C, respectively. The secondary peak off Mindanao Island is probably associated with the Mindanao Eddy, which causes significant mesoscale variability in SST and SLA.

The spatial structure of ISV of SLA is simulated well by the OFES model. Figure 7a shows the standard deviations of band-pass-filtered sea surface height, η, from the OFES model. The horizontal structure of ISV η in OFES output is similar to the satellite observed ISV of SLA in terms of magnitude and the pattern of southward decreasing gradients along the Philippine coast.

However, the distribution of *EKE* is quite different from the standard deviations of the intraseasonal SLA and η. We calculate the vertical mean *EKE* of the upper 250-m layer using 3-day OFES outputs. The OFES *EKE* generally decreases poleward from the equator (Figure 7b), which is consistent with the *EKE* time series observed by moored ADCPs (Figures 3 and 4). The maximum core of *EKE* with an amplitude greater than 100 $cm^2\ s^{-2}$, can be found in the equatorial region and in the coastal region east of the Philippines (Figure 7b). Thus, the spatial pattern of *EKE* is obviously different from that of the η.

Assuming that the upper layer currents in the Philippine Sea are in geostrophic balance, the horizontal pressure gradient, $\nabla\eta$, balances the Coriolis force. As a result, the assumption yields $|u| \propto \left|\frac{g}{f}\frac{\partial\eta}{\partial x_i}\right|$, and the spatial pattern in *EKE* is determined by the Coriolis force as well as the structure of η. To prove this hypothesis, we calculate the αSTD_η, where $\alpha = gf^{-1}\delta$, gravity $g = 9.8\ m\ s^{-2}$, f indicates the Coriolis factor, and δ denotes the order of horizontal gradient of η set as 10^{-7}, and STD_η is the standard deviation of η. Both the αSTD_η and *EKE* show relatively large values between 3 and 9°N and in the coastal band off the Philippines compared

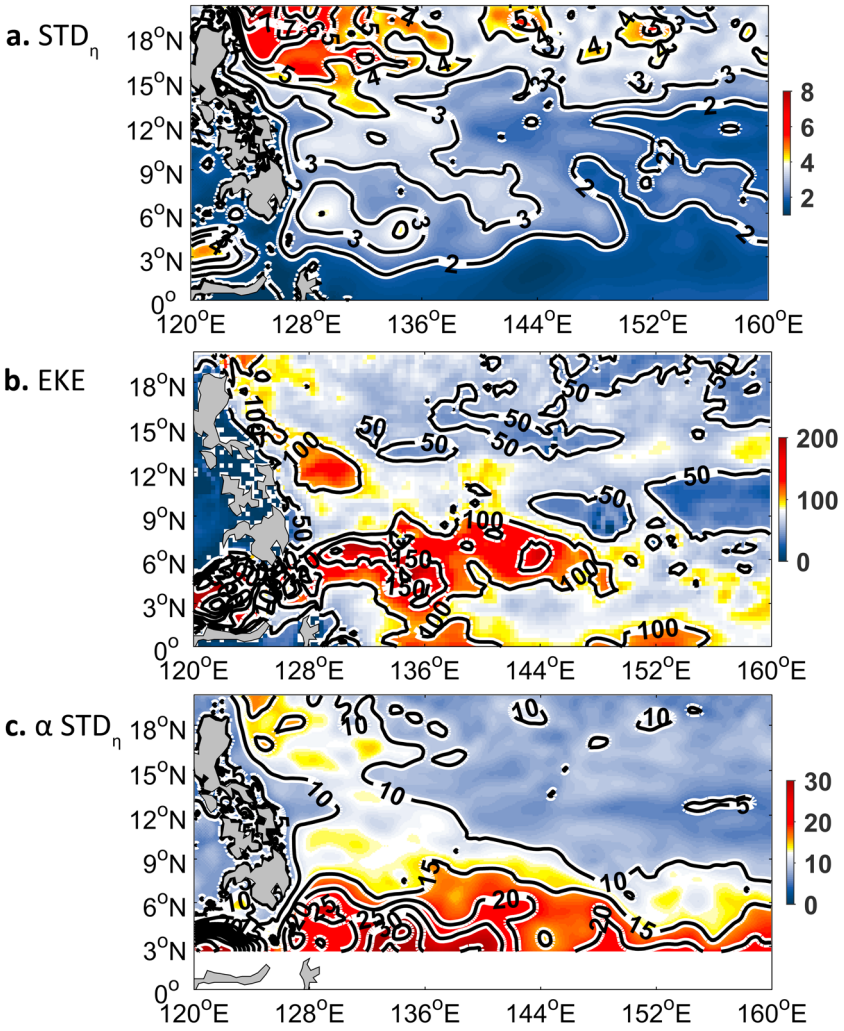

Figure 7. Spatial patterns of (a) standard deviations of OFES η (cm), (b) OFES *EKE* vertically averaged over the upper 250-m layer (cm^2 s^{-2}), and (c) αSTD_η (cm s^{-1}). OFES = OGCM for the Earth Simulator; *EKE* = eddy kinetic energy.

to other regions (Figure 7). This strongly suggests that the horizontal structure in *EKE* is determined by the sea surface height pattern and the Coriolis force.

Temporal structure of the upper layer intraseasonal variability is further investigated. The power spectra of *EKE* and volume transports observed by the moorings and SLA observed by satellites are calculated. Figure 8 presents a spectral map of latitude versus periods. A prominent feature is that the ISV periods are approximately symmetric about the equator and increase toward the poles. The spectra structure in *EKE* and volume transports is by and large similar to that of SLA. This is to be expected since the variability of *EKE* is from the same source as the SLA variability and the Coriolis force itself does not result in any temporal variability. Periods of *EKE* mainly fall in between about 40 to 60 days in the Philippine Sea, but SLA period shows a range between 48 and 74 days (Figure 8). Note that the SLA periods are nearly constant between about 6–12°N (i.e., the latitudes of the southern Philippine Sea). A latitude-period map of SLA periods averaged over 122–127.5°E (i.e., coastal region of the Philippine Sea) indicates a similar pattern as that found in Figure 8 (not shown), with a dominant period of around 51–53 days.

3.2. Sources of the Coastal ISV

Considering that the *EKE* shows a spatial pattern as a combination of SLA ISV and the Coriolis force, we suggest that the ISV of the upper layer current and SLA originate from the same source. The ISV of SLA is

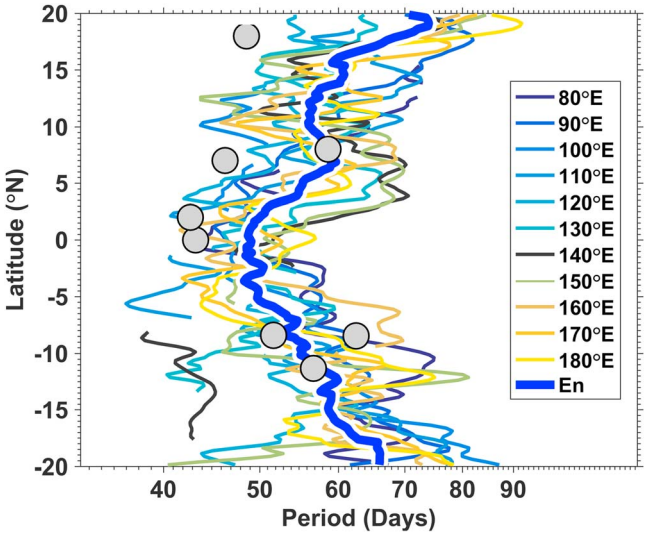

Figure 8. Meridional distribution of mean intraseasonal periods (days) of intraseasonal variabilities. Gray circles denote mooring observations averaged over the upper 300-m layer (M1–M5: eddy kinetic energy; M6–M8: Volume transport) and colorized lines indicates SLAs at various longitudes (see inset). The heavy blue line (*En*) indicates the ensemble mean of all the SLAs. SLA = sea level anomaly.

potentially influenced by local wind forcing and remote forcing through intraseasonal Rossby waves and mesoscale eddies. Lead-lag correlations show no significant relationship between ISV of SLA and local wind forcing (not shown).

The phase speeds of ISV of SLA are estimated using a Radon Transform of the longitude-time map of intraseasonal SLA along 8, 14, and 18°N (Figure 9). We find that the phase speeds at 8, 14, and 18°N are 23, 19, and 11 cm/s, respectively. The result is in agreement with the estimates of baroclinic Rossby waves at these latitudes (Chelton & Schlax, 1996), implying that the main form of intraseasonal SLA propagation is baroclinic Rossby waves and/or mesoscale eddy propagation.

Surface mesoscale eddies propagate westward with a speed close to the phase speed of baroclinic Rossby waves (Qiu & Chen, 2010) and cause intraseasonal fluctuations of SLA in the Philippine Sea. Hence, the distribution of mesoscale eddies could also play a role in determining the ISV pattern. Using the OFES outputs of horizontal currents velocity and sea surface height η, we tracked the simulated mesoscale eddies during 2011–2013 following the method of Yang et al., 2013. Figure 10 presents the number intensity of anticyclonic eddies and cyclonic eddies in the low-latitude western Pacific Ocean. Both anticyclonic eddies and cyclonic eddies are more numerous and stronger in the northern Philippine Sea compared to the south, even though the eddy intensity south of 8°N is also very high. Hence, the eddy distribution is similar to the spatial pattern of ISV of SLA, implying that the spatial distribution of mesoscale eddies contributes to the ISV of SLA.

Besides the zonal propagation of ISV signals, another important feature is the meridional propagation along the Philippine coast. Hovmöller diagrams of coastal and intraseasonal temperature anomaly and SLA along the Philippine coast are plotted in Figure 11. Phase lag and southward coastal propagation are quite clear along the Philippine coast, especially south of 12°N. We estimate the phase speed of the temperature anomaly and SLA along the coast using the Radon Transform and find that the ISV signals of SLA and temperature

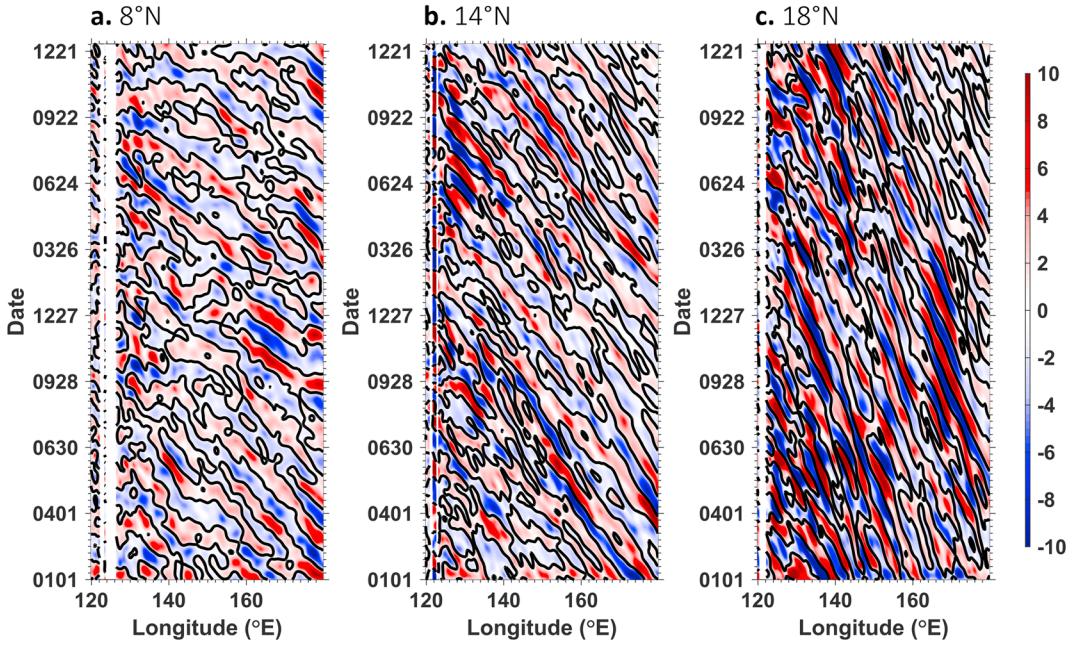

Figure 9. Daily sea level anomaly (cm) along (a) 8, (b) 14, and (c) 18°N from satellite observations. A 20- to 90-day band-pass filter is used to extract the intraseasonal variability signals.

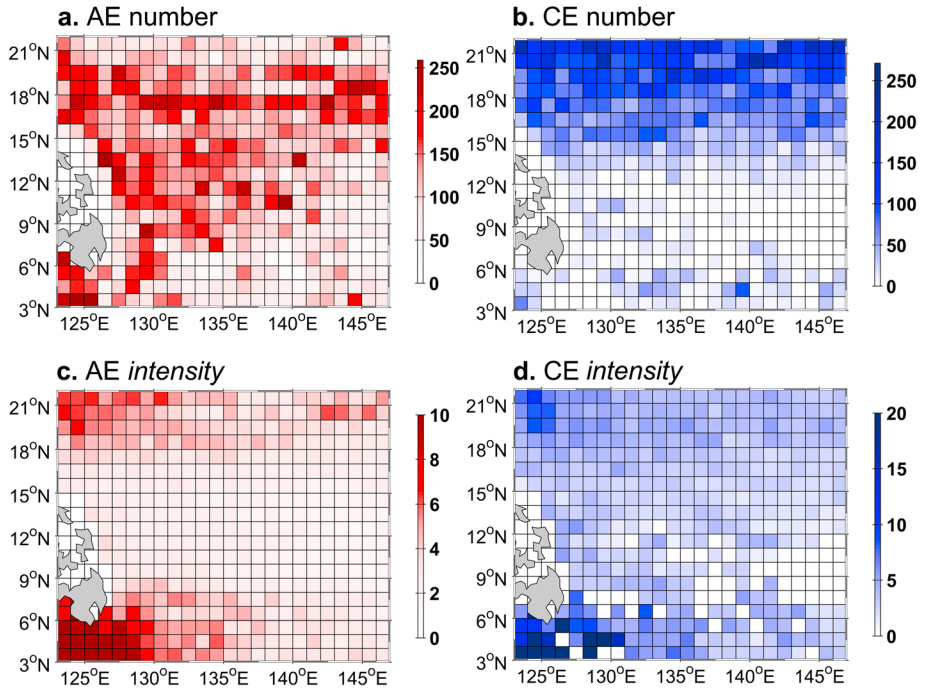

Figure 10. Number and intensity (unit in $10^{-3} \cdot cm^{-2} \cdot km^{-2}$) of (left) anticyclonic eddies (AEs) and (right) cyclonic eddies (CEs) in the low-latitude western Pacific Ocean during 2011–2013.

propagate southward with a speed of about 43 and 35 cm s^{-1} respectively. This is consistent with the southward propagation speed of coastal Kelvin waves (e.g., Beletsky et al., 1997). The coastal Kelvin waves transfer ISV signals southward and explains the observed significant coastal ISV SLA. Evidence of the presence of coastal Kelvin waves can be found in the meridional distribution of ISV periods: in contrast to other latitude bands, the ISV periods in the coastal region of the southern Philippine Sea (6–12°N) have a near-constant meridional gradient, consistent with coastal Kelvin waves that would not show changes in the frequency of ISVs along the Kelvin wave pathway.

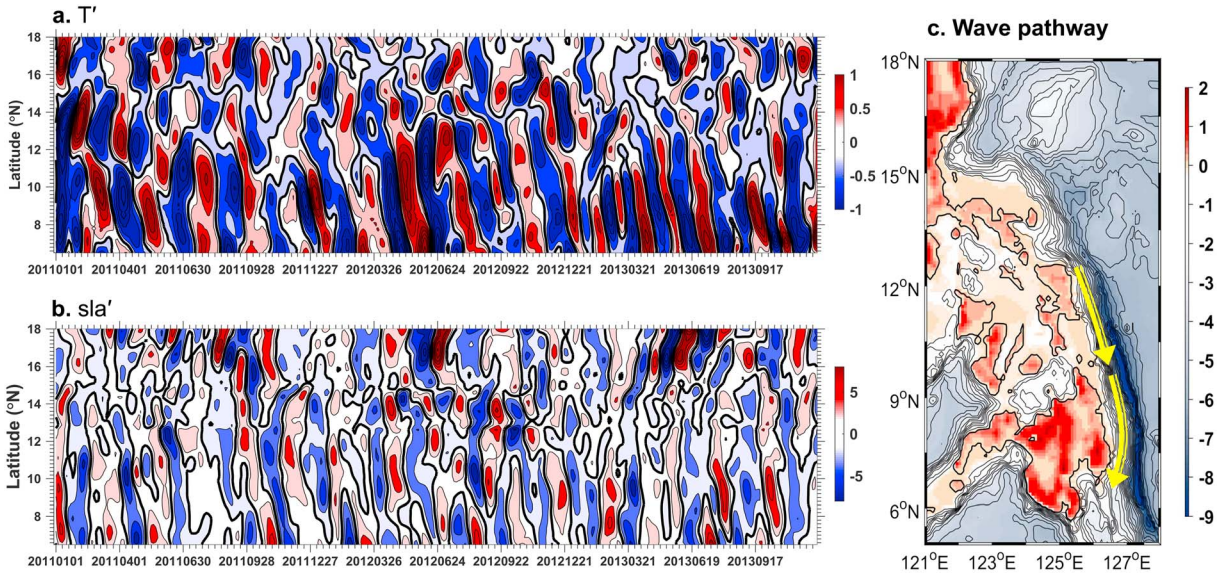

Figure 11. Coastal intraseasonal variabilities of (a) OGCM for the Earth Simulator temperature anomaly (°C) at 100 m and (b) satellite observed intraseasonal sea level anomaly (cm) to the east of the Philippine Islands during 2011–2013. Panel (c) shows the topography and a schematic pathway of the coastal Kelvin wave propagation along the Philippine coast.

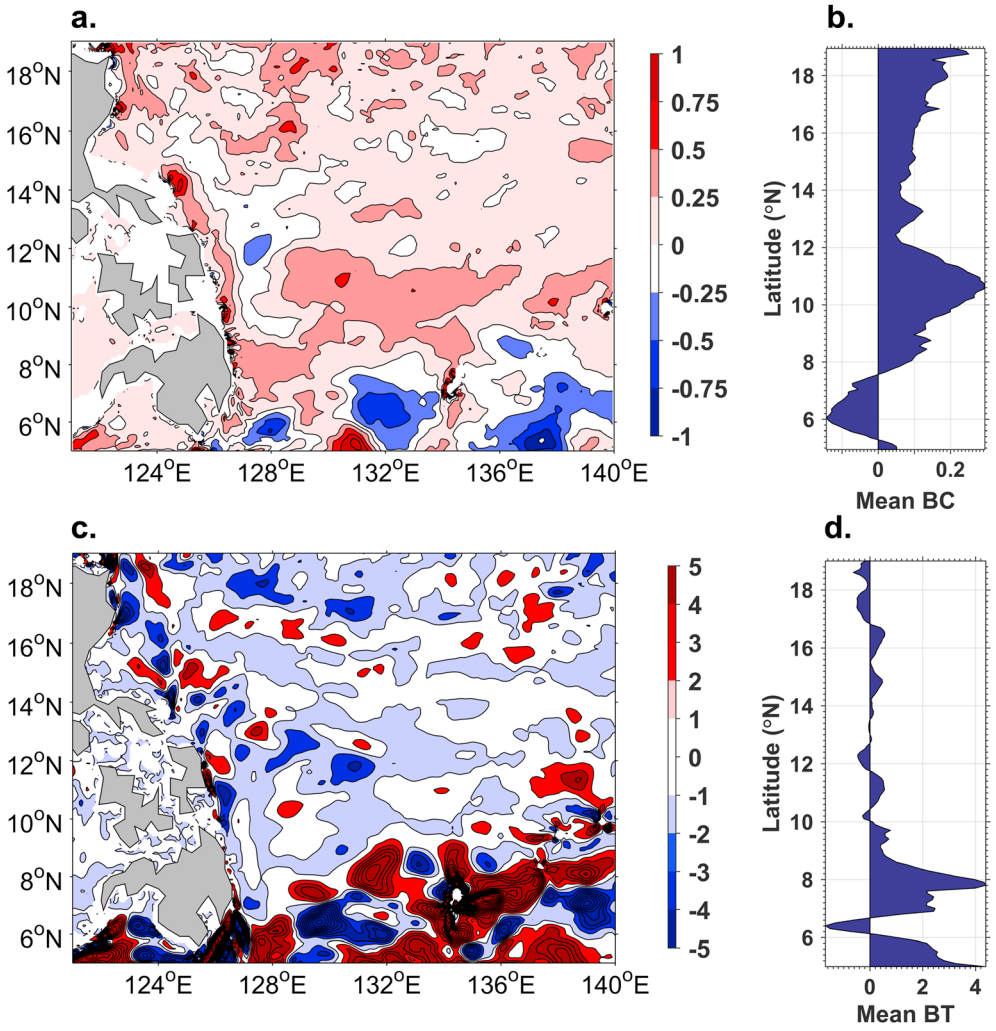

Figure 12. Annual mean (a) baroclinic conversion rate (BC, $10^{-8} \cdot m^2 \cdot s^{-3}$) and (c) barotropic conversion rate (BT, $10^{-8} \cdot m^2 \cdot s^{-3}$) calculated using OGCM for the Earth Simulator outputs. Right panels show a zonal mean (b) BC and (d) BT.

Baroclinic and barotropic instabilities are major energy sources for the oceanic eddies and hence ISVs. The conversion from eddy potential energy to *EKE* acts as the source for baroclinic instability, and the conversion from mean kinetic energy to *EKE* provides energy for barotropic instability. Following Qiu2015, we calculated the baroclinic and barotropic eddy energy conversion rate in the upper 250-m layer. The baroclinic conversion rate (BC) and the barotropic conversion rate (BT) are defined by

$$BC = -\frac{g}{\rho_0}\left(\overline{\rho' w'}\right) \tag{1}$$

$$BT = -\left(\overline{u_i' u_j'}\right)\frac{\partial \overline{u_i}}{\partial \overline{x_j}} \tag{2}$$

where ρ' and w' are potential density and vertical velocity anomalies from means over 2011–2013 and ρ_0 is set as 1,025 kg m^{-3}.

Figure 12 shows the time mean *BC* and *BT* in the upper layer from the 3-day OFES outputs. The spatial patterns of *BC* and *BT* are similar to that shown in Qiu2015. *BC* is clearly positive along the northern Philippine coast to about 8°N and negative in the south (Figures 12a and 12b). *BT* is mainly negative along the Philippine coast but positive in the southeastern Philippine Sea. The spatial patterns of *BC* and *BT* suggest that the release of mean available potential energy contributes to the mesoscale *EKE* and further contributes to

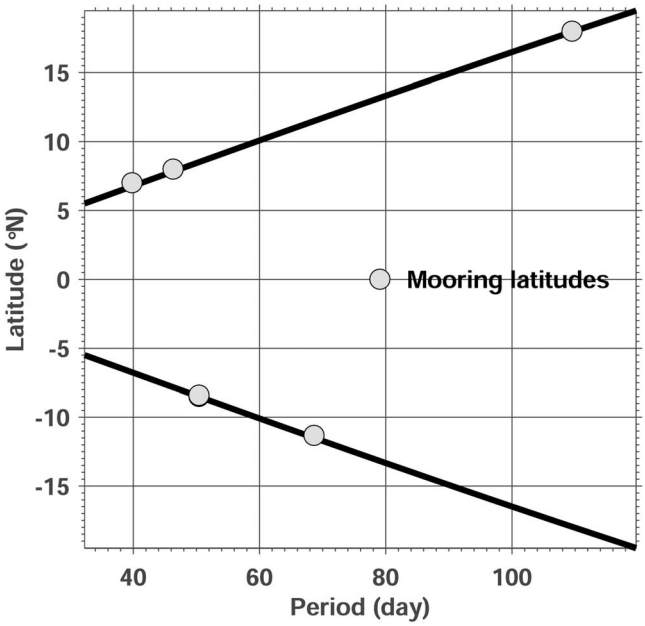

Figure 13. Latitudinal distribution of the theoretical period (black lines) from a linear baroclinic Rossby wave model. Gray cycles denote latitudes of moorings outside the 5° equatorial region.

the mean flow in the northern Philippine Sea, especially within the coastal region. In contrast, the mean kinetic energy contributes to the *EKE* and causes change in the potential energy. This suggests that the mean flow within the North Equatorial Countercurrent acts to generate mesoscale eddies through its strong meandering and further causes the SLA fluctuation in the southeastern Philippine Sea. Therefore, *BC* and *BT* rates determine the spatial distribution of mesoscale eddies and exert control over the horizontal patterns of ISV of SLA and *EKE*.

The Rossby wave-mesoscale eddy theory is also appropriate for interpreting the meridional distribution of ISV frequency observed by moorings and satellite SLA shown in Figure 8. Considering a traveling baroclinic Rossby wave, the dispersion relation is

$$\omega = \frac{\beta k}{k^2 + l^2 + L_d^{-2}} \tag{3}$$

where k and l are wave numbers and L_d is baroclinic deformation radius that is defined as $L_d = \sqrt{g' h_0}/f$. The mean layer depth h_0 is set as 250 m and reduced gravity acceleration is $g' = 0.03$ m s^{-2}. The wave period is hence

$$T = \frac{2\pi}{\omega} = \frac{2\pi\left(k^2 + l^2 + L_d^{-2}\right)}{\beta k}. \tag{4}$$

Assuming that $l = 0$ and $k = L_d^{-1}$, then the wave period is simplified to be

$$T \approx \frac{4\pi}{\beta L_d}. \tag{5}$$

We plot the period as a function of latitude in Figure 13. Clearly, the ISV period is symmetrical about the equator and increases poleward with latitude. This meridional pattern is similar to that of the observations (Figure 8).

Therefore, we suggest that the dynamic instability provides eddy energy for the intraseasonal mesoscale processes including mesoscale eddies and intraseasonal Rossby waves, leading to significant intraseasonal variability in SLA and the upper layer ocean currents through adjustment from the beta effect (Figure 14). Coastal Kelvin waves detected along the southern coast of the Philippine Sea cause a part of the intraseasonal fluctuations of western boundary SLA and currents. ISV in the Indonesian seas is mainly be related to coastal Kelvin waves forced in the Indian Ocean (e.g., Drushka et al., 2010) and is quite different from the ISV observed in the Philippine Sea.

3.3. Discussion: The Role of the MJO

Besides the role of internal oceanic dynamics in controlling the intraseasonal variability, atmospheric forcing at the sea surface related to the MJO potentially also plays a role in triggering the intraseasonal oceanic variability (e.g., Wang et al., 2016). Sea surface wind forcing and OLR show significant intraseasonal variation within the Indo-Pacific region, especially over the Philippine Sea (Figure 15). During the development and propagation of the MJO, the Indo-Pacific feels clear influence of the coupled wind-precipitation system at the ocean surface.

To investigate the oceanic response to the MJO forcing, we composite the SLA over various MJO phases indicated by the Real-time Multivariate MJO index (Figure 16). Significant positive SLA response to the MJO can be seen during phases 1 and 8 east of the Luzon Island, and phase 7 at latitude of about 5°N. Significant negative SLA response is seen during phases 2 to 7 in the Philippine Sea that is maximum in the north. The MJO-induced SLA variation is about 1 to 3 cm, with maxima in the northern and middle Philippine Sea (Figure 16i). Clearly, the spatial pattern of the MJO-induced SLA variation (Figure 16i) is similar to the observed intraseasonal SLA variation (Figure 6b). However, the amplitude of MJO-induced SLA variation in the Philippine Sea is

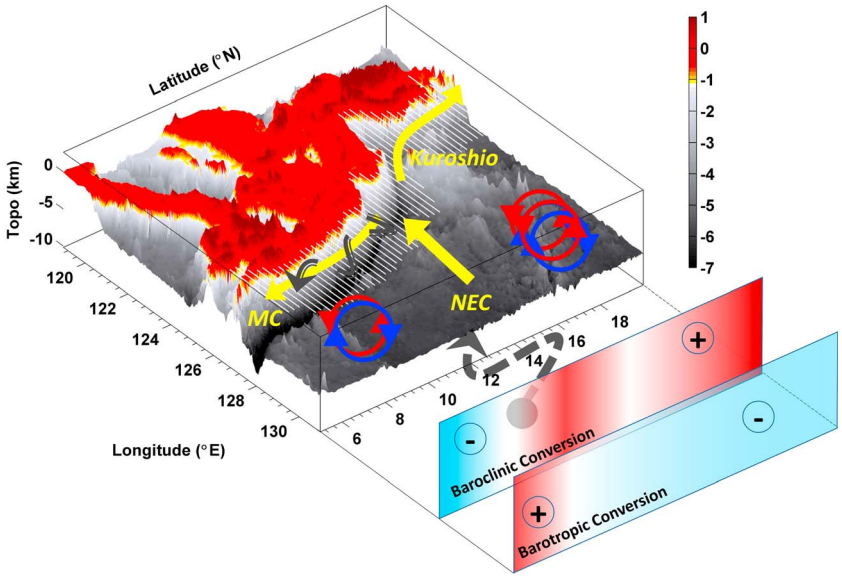

Figure 14. Schematic of the physical processes determining the coastal intraseasonal variability in the Philippine Sea. Baroclinic and barotropic conversions provide energy for mesoscale eddies (red and blue arrows) and intraseasonal Rossby waves (gray dashed arrow lines) and further leads to intraseasonal variability in the Philippine Sea. Coastal Kelvin waves (gray dashed arrow lines along the coast) links the intraseasonal variabilities in the southern coastal region. NEC = North Equatorial Current; MC = Mindanao Current.

less than but close to about half of the total ISV of SLA, implying that the surface MJO forcing plays an important but not dominant role in determining the oceanic intraseasonal variability in the Philippine Sea. Previous studies have suggested that the MJO-related wind stress forcing gives rise to significant Ekman transport and sea surface height fluctuation near the equator (e.g., Marshall & Hendon, 2014). This MJO-induced forcing leads to significant intraseasonal fluctuation of the surface meridional current in the Philippine Sea (Marshall & Hendon, 2014).

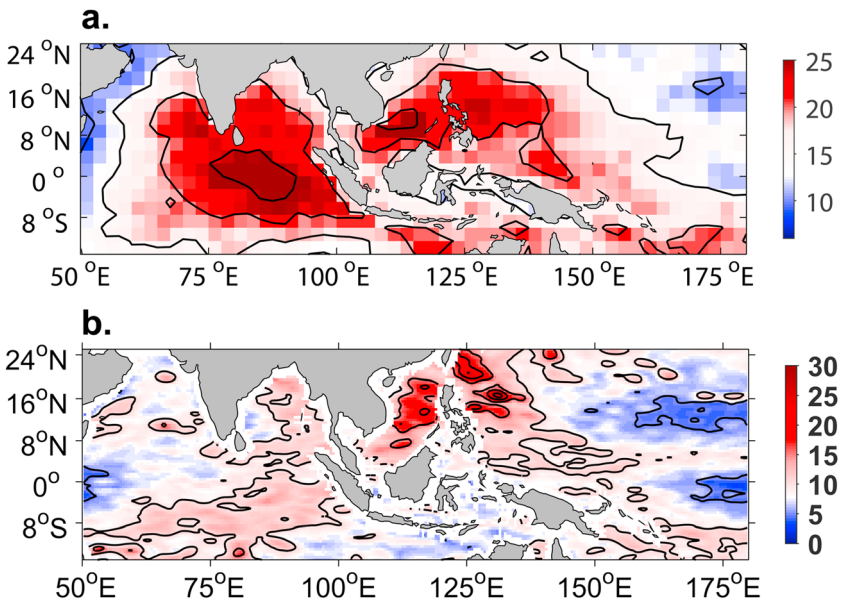

Figure 15. Standard deviations of intraseasonal variabilities of (a) outgoing long-wave radiation anomaly (W m^{-2}) and (b) QuikSCAT wind stress curl anomaly (10^{-8} Pa m^{-1}) over the tropical Indo-Pacific Ocean during 2006–2008.

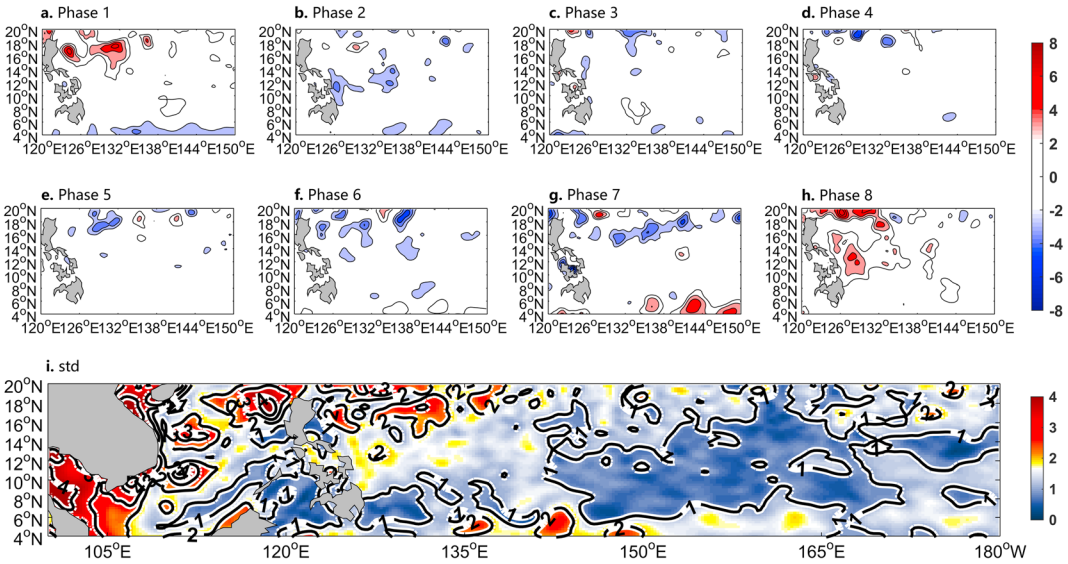

Figure 16. MJO composited AVISO SLAs (a–h, cm) based on the Real-time Multivariate MJO index and standard deviation of SLA induced by MJO cycle (i, cm). MJO = Madden-Julian Oscillation; SLA = sea level anomaly.

Acknowledgments

AVISO sea level data can be found at http://www.aviso.oceanobs.com/duacs/. OFES outputs are provided by the Japan Agency for Marine-Earth Science and Technology and distributed by the Asia-Pacific Data Research Center at http://apdrc.soest.hawaii.edu/dods/public_ofes/OfES. NPOCE mooring data can be found at a repository site at zenodo (doi: 10.5281/zenodo.1257516). JAMSTEC mooring data can be found at http://www.jamstec.go.jp/rigc/j/tcvrp/ipocvrt/adcp_data.html. RG Argo data are provided by the Scripps Institution of Oceanography at University of California San Diego (http://sio-argo.ucsd.edu/RG_Climatology.html). RMM index is provided by NOAA/CPC at www.cpc.ncep.noaa.gov/products/precip/CWlink/MJO. Shijian Hu was jointly supported by the National Natural Science Foundation of China (41406016 and 41776018), the Key Research Program of Frontier Sciences, CAS (QYZDB-SSW-SYS023), the Open Fund of State Key Laboratory of Satellite Ocean Environment Dynamics, Second Institute of Oceanography (QNHX1601), and Open Fund of the Key Laboratory of Ocean Circulation and Waves, Chinese Academy of Sciences (KLOCW1801). Dunxin Hu and Fan Wang were supported by the National Natural Science Foundation of China (41330963 and 41730534). Janet Sprintall was supported by NOAA's Climate Program Office, Climate Variability and Predictability Program (award NA17OAR4310257). Cong Guan was supported by the China Postdoctoral Science Foundation (2017M622289). Discussion with Cesar Villanoy and Bo Qiu are helpful. We are grateful to Kentaro Ando and Hideharu Sasaki for providing access to the TRITON data and OFES outputs.

4. Summary

The Philippine Sea is characterized by striking intraseasonal variability due to the intersection of mesoscale oceanic eddies and waves in the northwestern Pacific Ocean and significant forcing associated with the eastward propagation of the MJO. ISV is thought to be the key in bridging the weather and climate system. In this paper, we examined the spatial structure of intraseasonal oceanic variability in the Philippine Sea with a focus along the coast combining multisource in situ and remote observations and OFES model outputs. Major results are evident in three aspects.

First of all, the ISV of SLA intensity decreases from the northern and coastal Philippine Sea to the southern and interior Pacific Ocean. In contrast, the *EKE* features a northward decreasing gradient with a maximum at about 6°N. The meridional distribution of SLA and *EKE* spectra indicates a linear increase of ISV periods with latitude that is symmetrical about the equator.

Second, westward propagating mesoscale eddies and Rossby waves related to dynamic instability are found to be an important source of the oceanic ISV in the Philippine Sea. Under the influence of the β effect, the mesoscale eddies and Rossby waves explain the spatial and temporal patterns of oceanic ISV. Clear coastal propagation of ISVs related to coastal Kelvin waves is detected south of about 14°N.

Finally, composite analysis shows that the MJO provides another important forcing of oceanic ISV, forming the spatial patterns along the Philippine coast and contributing about half of the total observed intraseasonal signal of SLA.

Nonetheless, issues remain. The specific processes through which the MJO influences the ISVs in the Philippine Sea is unclear. The role of the significant oceanic ISV in the climate system need further studies. For example, the Philippine Sea is an important region in the development of the distinct meridional gradients evident in the western Pacific warm pool SST that are caused by anomalous oceanic upwelling during El Niño events (Hu et al., 2017). Whether and how the oceanic ISV in the Philippine Sea might affect this warm pool phenomena and act to rectify and intensify the associated El Niño events is still an unanswered question.

References

Beletsky, D., O'Connor, W. P., Schwab, D. J., & Dietrich, D. E. (1997). Numerical simulation of internal Kelvin waves and coastal upwelling fronts. *Journal of Physical Oceanography*, *27*(7), 1197–1215. https://doi.org/10.1175/1520-0485(1997)027<1197:nsoikw>2.0.co;2

Chelton, D. B., & Schlax, M. G. (1996). Global observations of oceanic Rossby waves. *Science*, *272*(5259), 234–238. https://doi.org/10.1126/science.272.5259.234

Dibarboure, G., Lauret, O., Mertz, F., & Rosmorduc, V. (2009). SSALTO/DUACS user handbook:(M) SLA and (M) ADT near-real time and delayed time products, *Rep*. CLS-DOS-NT, 6, 51.

Drushka, K., Sprintall, J., Gille, S. T., & Brodjonegoro, I. (2010). Vertical structure of Kelvin waves in the Indonesian throughflow exit passages. *Journal of Physical Oceanography*, *40*(9), 1965–1987. https://doi.org/10.1175/2010jpo4380.1

Gilson, J., & Roemmich, D. (2002). Mean and temporal variability in Kuroshio geostrophic transport south of Taiwan (1993–2001). *Journal of Oceanography*, *58*(1), 183–195. https://doi.org/10.1023/A:101584112

Gray, A. R., & Riser, S. C. (2014). A global analysis of Sverdrup balance using absolute geostrophic velocities from Argo. *Journal of Physical Oceanography*, *44*(4), 1213–1229. https://doi.org/10.1175/JPO-D-12-0206.1

Hu, D., Hu, S., Wu, L., Li, L., Zhang, L., Diao, X., et al. (2013). Direct measurements of the Luzon undercurrent. *Journal of Physical Oceanography*, *43*(7), 1417–1425. https://doi.org/10.1175/JPO-D-12-0165.1

Hu, D., Wang, F., Wu, L., Chen, D., Liu, Q., Tian, J., et al. (2011). *Northwestern Pacific Ocean Circulation and Climate Experiment (NPOCE) science/implementation plan* (p. 100). Beijing: China Ocean Press.

Hu, D., Wu, L., Cai, W., Gupta, A. S., Ganachaud, A., Qiu, B., et al. (2015). Pacific western boundary currents and their roles in climate. *Nature*, *522*(7556), 299–308. https://doi.org/10.1038/nature14504

Hu, S., Hu, D., Guan, C., Wang, F., Zhang, L., Wang, F., & Wang, Q. (2016). Interannual variability of the Mindanao Current/Undercurrent in direct observations and numerical simulations. *Journal of Physical Oceanography*, *46*(2), 483–499. https://doi.org/10.1175/JPO-D-15-0092.1

Hu, S., Hu, D., Guan, C., Xing, N., Li, J., & Feng, J. (2017). Variability of the western Pacific warm pool structure associated with El Niño. *Climate Dynamics*, *49*(7–8), 2431–2449. https://doi.org/10.1007/s00382-016-3459-y

Kashino, Y., Ishida, A., & Kuroda, Y. (2005). Variability of the Mindanao Current: Mooring observation results. *Geophysical Research Letters*, *32*, L18611. https://doi.org/10.1029/2005GL023880

Liebmann, B., & Smith, C. A. (1996). Description of a complete (interpolated) outgoing longwave radiation dataset. *Bulletin of the American Meteorological Society*, *77*(6), 1275–1277.

Lin, X., Wu, D., Li, Q., & Lan, J. (2005). An amplification mechanism of intraseasonal long Rossby wave in subtropical ocean. *Journal of Oceanography*, *61*(2), 369–378. https://doi.org/10.1007/s10872-005-0047-x

Liu, Q., Feng, M., & Wang, D. (2011). ENSO-induced interannual variability in the southeastern South China Sea. *Journal of Oceanography*, *67*(1), 127–133. https://doi.org/10.1007/s10872-011-0002-y

Madden, R. A., & Julian, P. R. (1971). Detection of a 40–50 day oscillation in the zonal wind in the tropical Pacific. *Journal of the Atmospheric Sciences*, *28*(5), 702–708. https://doi.org/10.1175/1520-0469(1971)028<0702:DOADOI>2.0.CO;2

Madden, R. A., & Julian, P. R. (1972). Description of global-scale circulation cells in the tropics with a 40–50 day period. *Journal of the Atmospheric Sciences*, *29*(6), 1109–1123. https://doi.org/10.1175/1520-0469(1972)029<1109:DOGSCC>2.0.CO;2

Marshall, A. G., & Hendon, H. H. (2014). Impacts of the MJO in the Indian Ocean and on the Western Australian coast. *Climate Dynamics*, *42*(3-4), 579–595. https://doi.org/10.1007/s00382-012-1643-2

McPhaden, M. J., Bourlès, B., Freitag, H. P., Lumpkin, R., Masumoto, Y., Murty, V. S. N., et al. (2009). The global tropical moored buoy array. In H. D. Hall, & D. Stammer (Eds.), *Proceedings of the OceanObs' 09:Sustained Ocean Observations and Information for Society Conference* (pp. 21–25). Venice, Italy: ESA publication WPP-306.

Qiu, B., & Chen, S. (2010). Interannual variability of the North Pacific subtropical countercurrent and its associated mesoscale eddy field. *Journal of Physical Oceanography*, *40*(1), 213–225. https://doi.org/10.1175/2009JPO4285.1

Qiu, B., Chen, S., Rudnick, D. L., & Kashino, Y. (2015). A new paradigm for the North Pacific subthermocline low-latitude western boundary current system. *Journal of Physical Oceanography*, *45*(9), 2407–2423. https://doi.org/10.1175/JPO-D-15-0035.1

Qu, T., Chiang, T. L., Wu, C. R., Dutrieux, P., & Hu, D. (2012). Mindanao Current/Undercurrent in an eddy-resolving GCM. *Journal of Geophysical Research*, *117*, C06026. https://doi.org/10.1029/2011JC007838

Reynolds, R. W., Smith, T. M., Liu, C., Chelton, D. B., Casey, K. S., & Schlax, M. G. (2007). Daily high-resolution-blended analyses for sea surface temperature. *Journal of Climate*, *20*(22), 5473–5496. https://doi.org/10.1175/2007jcli1824.1

Roemmich, D., & Gilson, J. (2009). The 2004–2008 mean and annual cycle of temperature, salinity, and steric height in the global ocean from the Argo Program. *Progress in Oceanography*, *82*(2), 81–100. https://doi.org/10.1016/j.pocean.2009.03.004

Roemmich, D., Johnson, G. C., Riser, S. C., Davis, R. E., Gilson, J., Owens, W. B., et al. (2009). The Argo program observing the global ocean with profiling floats. *Oceanography*, *22*(2), 34–43. https://doi.org/10.5670/oceanog.2009.36

Sasaki, H., Nonaka, M., Masumoto, Y., Sasai, Y., Uehara, H., & Sakuma, H. (2008). An eddy-resolving hindcast simulation of the quasiglobal ocean from 1950 to 2003 on the Earth Simulator. In *High resolution numerical modelling of the atmosphere and ocean* (pp. 157–185). New York: Springer.

Sprintall, J., Wijffels, S., Gordon, A. L., Ffield, A., Molcard, R., Susanto, R. D., et al. (2004). INSTANT: A new international array to measure the Indonesian Throughflow. *Eos, Transactions American Geophysical Union*, *85*(39), 369–376. https://doi.org/10.1029/2004EO390001

Sprintall, J., Wijffels, S. E., Molcard, R., & Jaya, I. (2009). Direct estimates of the Indonesian Throughflow entering the Indian Ocean: 2004–2006. *Journal of Geophysical Research*, *114*, C07001. https://doi.org/10.1029/2008JC005257

Wang, F., Li, Y., & Wang, J. (2016). Intraseasonal variability of the surface zonal currents in the western tropical Pacific Ocean: Characteristics and mechanisms. *Journal of Physical Oceanography*, *46*(12), 3639–3660. https://doi.org/10.1175/JPO-D-16-0033.1

Wang, Q., Zhai, F., & Hu, D. (2014). Variations of Luzon Undercurrent from observations and numerical model simulations. *Journal of Geophysical Research: Oceans*, *119*, 3792–3805. https://doi.org/10.1002/2013jc009694

Wang, Q., Zhai, F., Wang, F., & Hu, D. (2014). Intraseasonal variability of the subthermocline current east of Mindanao. *Journal of Geophysical Research: Oceans*, *119*, 8552–8566. https://doi.org/10.1002/2014JC010343

Wheeler, M. C., & Hendon, H. H. (2004). An all-season real-time multivariate MJO index: Development of an index for monitoring and prediction. *Monthly Weather Review*, *132*(8), 1917–1932. https://doi.org/10.1175/1520-0493(2004)132<1917:AARMMI>2.0.CO;2

Yang, G., Wang, F., Li, Y., & Lin, P. (2013). Mesoscale eddies in the northwestern subtropical Pacific Ocean: Statistical characteristics and three-dimensional structures. *Journal of Geophysical Research: Oceans*, *118*, 1906–1925. https://doi.org/10.1002/jgrc.20164

Zhang, C. (2013). Madden–Julian Oscillation: Bridging weather and climate. *Bulletin of the American Meteorological Society*, *94*(12), 1849–1870. https://doi.org/10.1175/BAMS-D-12-00026.1

Zhang, L., Hu, D., Hu, S., Wang, F., Wang, F., & Yuan, D. (2014). Mindanao Current/Undercurrent measured by a subsurface mooring. *Journal of Geophysical Research: Oceans*, *119*, 3617–3628. https://doi.org/10.1002/2013JC009693

Zhuang, W., Qiu, B., & Du, Y. (2013). Low-frequency Western Pacific Ocean sea level and circulation changes due to the connectivity of the Philippine Archipelago. *Journal of Geophysical Research: Oceans*, *118*, 6759–6773. https://doi.org/10.1002/2013JC009376